SCISPACE
formerly Typeset

Open access • Journal Article • DOI:10.1002/NAVI.178

Enhancing Least Squares GNSS Positioning with 3D Mapping without Accurate Prior Knowledge — Source link

Mounir Adjrad, Paul D. Groves

Institutions: University College London

Published on: 01 Mar 2017 - Annual of Navigation (John Wiley & Sons, Ltd)

Topics: GNSS applications and Ranging

Related papers:

- Multi-Constellation GNSS Performance Evaluation for Urban Canyons Using Large Virtual Reality City Models
- Smartphone Shadow Matching for Better Cross-street GNSS Positioning in Urban Environments
- 3D building model-based pedestrian positioning method using GPS/GLONASS/QZSS and its reliability calculation
- Shadow Matching: A New GNSS Positioning Technique for Urban Canyons
- About Non-Line-Of-Sight Satellite Detection and Exclusion in a 3D Map-Aided Localization Algorithm

Share this paper:

View more about this paper here: https://typeset.io/papers/enhancing-least-squares-gnss-positioning-with-3d-mapping-a6kyc6bdp1

Enhancing Least Squares GNSS Positioning with 3D Mapping without Accurate Prior Knowledge

MOUNIR ADJRAD and PAUL D. GROVES

University College London, London, UK

ABSTRACT: Global Navigation Satellite System (*GNSS*) *positioning performance in dense urban areas is severely degraded due to the obstruction and reflection of the signals by the surrounding buildings. A basic GNSS position solution can exhibit errors of tens of meters, sometimes more. Here 3D mapping is used to aid conventional ranging-based GNSS positioning. Terrain height-aiding is used to contribute an additional virtual ranging measurement to the position solution. In addition, 3D city models are used to predict Non-Line-Of-Sight (NLOS) reception over a large search area. The resulting NLOS probabilities are used to aid a consistency checking algorithm that selects and weights the signal used for the final position solution. Iteration is employed to refine the position solution. Practical test results demonstrate improvement in the horizontal and vertical accuracy of conventional ranging-based GNSS positioning in urban areas by a factor of 2.5 and 5, respectively. Using the new technique, the Root Mean Square (RMS) position error in dense urban areas was found to be 20.8m horizontally and 12.2m vertically.*

KEY WORDS: Height-Aiding, Consistency Checking, Urban Canyons, Intelligent Urban Positioning.

INTRODUCTION

Improving upon the relative poor real-time positioning accuracy achievable in dense urban areas can unlock the potential for a host of new positioning applications. Examples include navigation for the visually impaired, tracking people with chronic medical conditions and emergency caller location. For these latter applications, it is important to determine which side of the street a pedestrian is on and which building they are in front of. This is also useful for guiding visitors, meeting friends and business associates and location-based advertising, while augmented reality relies on knowing where the user is. Similarly, to make best use of the space in cities, sustainable transport requires advanced lane control systems for vehicles and advanced railway signaling systems, both of which require accurate positioning. With the emergence of citizen science, low-cost devices to measure noise and pollution are becoming prevalent. As these measurements vary greatly across a street, accurate positioning is required to interpret the results.

The Global Positioning System (GPS) provides meters-level positioning in open environments, but the accuracy and reliability in urban areas is poor because buildings block, attenuate, reflect and diffract radio signals. This has conventionally been a major hindrance to positioning, with errors of tens of meters common and often no position solution available at all [1]. Using the new Global Navigation Satellite Systems (GNSS) constellations (GLONASS and, in future, Galileo and Compass) in addition to GPS dramatically increases the number of usable satellites. This improves the availability of a position solution in urban areas, but not the accuracy [2].

One way of improving positioning performance is to integrate GNSS with dead reckoning (DR) sensors, such as low-cost inertial sensors and car odometers [3]. DR sensors measure change in position, so require a good GNSS position solution for initialization. Following this,

their positioning errors increase over time, so they are only useful for bridging short gaps in GNSS coverage. Another approach is to use other widely available radio signals, such as Wi-Fi, phone signals, and television. However, these typically suffer from the same propagation errors as GNSS in urban environments so do not offer better accuracy. Visual techniques are another option. However, they require extensive processing and data storage capacity and can be sensitive to passing pedestrians and vehicles, and variation in lighting.

Reliable meters-level positioning in dense urban areas is almost impossible to achieve cost-effectively using a single method. To achieve this goal, a paradigm shift is needed. Instead of designing a single-technology navigation or positioning system, we need to use as much information as we can cost-effectively obtain from many different sources in order to determine the best possible navigation solution in terms of both accuracy and reliability.

This new approach to navigation and real-time positioning in challenging environments requires many new lines of research to be pursued [4]. These include:

- How to integrate many different navigation and positioning technologies when the necessary expertise is spread across multiple organizations [5];
- How to adapt a multisensor navigation system in real-time to changes in the environmental and behavioral context to maintain an optimal solution [6];
- How to obtain more information for positioning by making use of new features of the environment [7];
- How to use 3D mapping to improve the performance of existing positioning technologies, such as GNSS, in dense urban areas.

The final item is the subject of the present paper. Intelligent urban positioning (IUP) aims to achieve a step change in the performance of real-time GNSS positioning in dense urban areas by combining three key ingredients [8]:

- Multi-constellation GNSS;

- New techniques for detection of non-line-of-sight (NLOS) signal propagation;
- Three-dimensional mapping.

Making use of the signals from all visible GNSS satellites significantly increases the amount of information available to compute a position solution from. It also provides the flexibility to select which signals to use and which to discard. NLOS signals are received only via reflected surfaces and can contribute large ranging errors. If these signals can be identified and excluded [9, 10], the accuracy of conventional GNSS positioning may be substantially improved. Therefore, multi-constellation GNSS and effective NLOS detection are both critical components of any initiative to improve GNSS positioning accuracy in challenging urban environments.

There are at least three ways in which 3D mapping can be used to enhance GNSS positioning: detection and mitigation of NLOS reception, shadow matching and height-aiding. A full IUP implementation would incorporate all three of these techniques and could also use conventional map matching [11].

A number of research groups have shown that 3D city models can be used to mitigate the effects of NLOS GNSS signal reception, a major source of error in dense urban areas. The 3D model can be used to predict which signals are NLOS and exclude these from the position solution, which is otherwise computed using conventional ranging-based GNSS positioning.

There are a number of different ways in which this could be done, as illustrated in Figure 1. A single candidate position may be considered if the location is already roughly known, whereas multiple candidate positions must be considered if the positioning uncertainty is several tens of meters, which increases the processing load. The 3D city model can also be used merely to predict whether a signal is NLOS or it can be used to predict the range correction required to use reflected signals for positioning. Again, predicting the range corrections requires substantially more processing capacity.

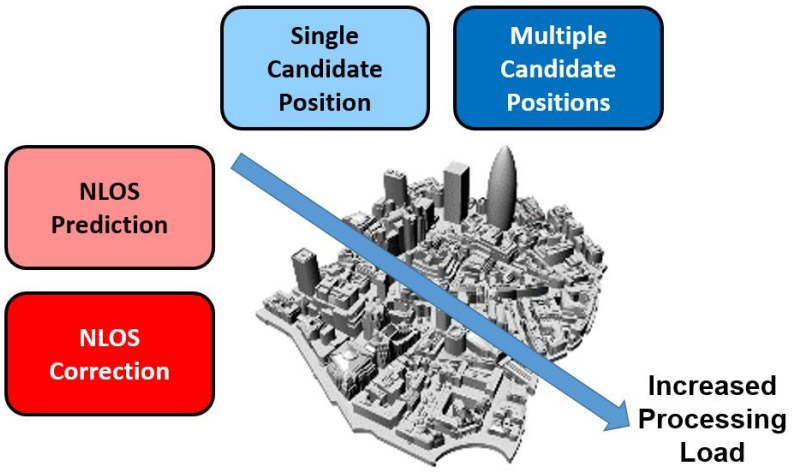

Fig. 1-Ways of aiding conventional ranging-based GNSS positioning using 3D models.

Early implementations assumed that the position was approximately known [12, 13]. Using the 3D model to correct the NLOS ranging errors takes this a stage further [14]. However this does not work when the initial position uncertainty is several tens of meters because different satellites are visible at different positions within the area in which the user may be located. Therefore, several research groups have extended the concept of 3D-mapping-aided GNSS ranging by using the 3D city model to predict the path delay of the NLOS signals across a range of candidate positions [15-18]. A single-epoch positioning accuracy of 4m has been reported [18]. However, the path delay must be determined using ray tracing, which is highly computationally intensive and thus an obstacle to real-time implementation if the search area is large. The urban trench approach [19] enables the path delays of NLOS signals to be computed very efficiently, but only if the building layout is highly symmetric.

The challenge is to develop a computationally efficient NLOS mitigation technique that can cope with position uncertainties of tens of meters. We therefore predict NLOS signal reception across a wide area and use this to aid signal selection and weighting within the positioning algorithm. We do not attempt to predict the path delay. This enables us to use pre-computed building boundaries [2] to predict satellite visibility very rapidly simply by comparing the

satellite elevation with that of the building boundary at the corresponding azimuth at each candidate position.

The second way of aiding GNSS using 3D mapping is shadow matching. This is a new technique that determines position by comparing the measured signal availability and strength with predictions made using a 3D city model [20]. It is designed to be used alongside conventional ranging-based GNSS positioning in dense urban areas in order to improve the cross-street accuracy. Since 2011, several groups have demonstrated shadow matching experimentally, using both single and multiple epochs of GNSS data [21-25]. Cross-street positions within a few meters have been achieved in environments where the error in the conventional GNSS position solution is tens of meters, enabling users to determine which side of the street they're on. Shadow matching has also been demonstrated in real time on an Android smartphone [26]. The challenge now is to improve reliability and integrate shadow matching with other positioning techniques [27].

The third way in which 3D mapping may be used to aid GNSS is terrain height-aiding. This may be used to generate a virtual ranging measurement [28] which substantially improves the solution geometry in dense urban environments, improving horizontal as well as vertical positioning using ranging based GNSS. The terrain height is also used in shadow matching to find the candidate position.

Our overall aim is to combine all three types of aiding from 3D mapping into GNSS positioning: height-aiding, NLOS mitigation and shadow matching. However, this paper focuses primarily on the use of 3D mapping to aid ranging-based GNSS positioning, namely assisting the signal selection and weighting within the positioning algorithm and terrain height-aiding. The methodology is described first. The results achieved using GPS and GLONASS data collected in London are then presented, followed by a summary of the conclusions and

future work. This article is partially based on a paper presented at ION GNSS+ 2015 in Tampa, FL [29].

APPROACH

Our approach uses spatial data in two different ways. Firstly, building boundary data derived from a 3D city model is used to assist the signal selection and weighting within the positioning algorithm. The building boundaries are used to predict if each signal is directly receivable over a range of candidate positions centered on an approximate GNSS position solution [2]. This approach is much faster than using the city model directly though building boundaries can use more memory. From this, the probability of each signal being NLOS or directly received is then estimated. This was combined with consistency checking, signal geometry and signal strength information, based on previous work performed at University College London (UCL), to predict which combination and weighting of signals produces the best position solution [30].

Our second technique uses Digital Terrain Models (DTMs) to aid GNSS positioning by effectively providing an additional ranging measurement. Previous research with simulated height-aiding showed that this has the potential to improve horizontal as well as vertical positioning in dense urban environments through improved solution geometry [30]. Here, height-aiding is provided from a real DTM with interpolation and iteration used to maximise the precision. This is described in the Terrain Height-Aiding sub-section.

Figure 2 shows the enhanced GNSS ranging algorithm, comprising six steps. The following steps are iterated several times to improve the position solution.

- A search area is determined using the conventional GNSS position solution on the first iteration and the previous solution on subsequent iterations, together with an appropriate confidence interval.

- Using the building boundaries precomputed from the 3D city model, the proportion of the search area within which each satellite is directly visible is computed, providing an estimate of the probability that the signal is direct LOS.
- A consistency checking process is applied as described in [30] with the additional use of the direct LOS probabilities from the 3D mapping at different stages of the algorithm.
- The set of signals resulting from the consistency checking process is subjected to a weighting strategy exploiting the previously determined LOS probabilities, satellite elevation and C/N0.
- DTM information is extracted from the 3D city model and a virtual range measurement is generated using the position at the center of the search area.
- Finally, a position solution is derived from a modified least-squares estimation process.

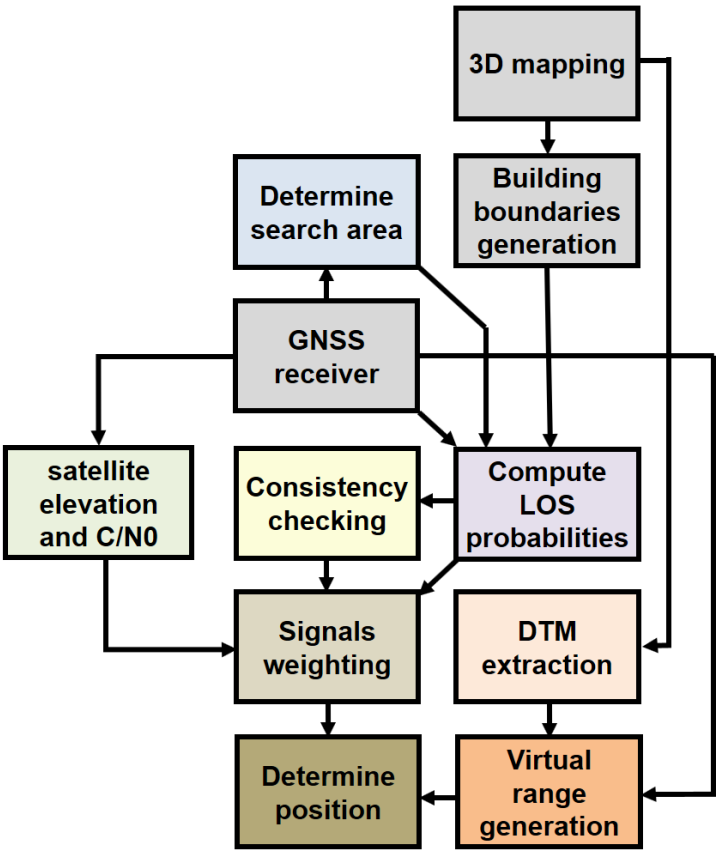

Fig. 2- Enhanced GNSS ranging algorithm block diagram.

3D Modelling

In March 2014 Ordnance Survey (OS) published an alpha release of the Building Height Attribute (BHA) dataset, which is an enhancement to OS MasterMap Topography Layer [31]. The first alpha release of BHA included buildings covering approximately 8,000km^2 of the United Kingdom (UK). Subsequent releases have increased the coverage of the dataset which covers major towns and cities in Great Britain. A number of attributes are provided for each building, as shown in Figure 3, these are:

- AbsHMin: The height of the ground level with respect to the vertical datum;
- AbsH2: The height of the base of the roof with respect to the vertical datum;
- AbsHMax: The height of the highest part of the roof with respect to the vertical datum;
- RelHMax: The relative height from ground level to the highest part of the roof;
- RelH2: The relative height from ground level to the base of the roof.

RelH2 was used here as it provides a good representation of the height of buildings relative to one another.

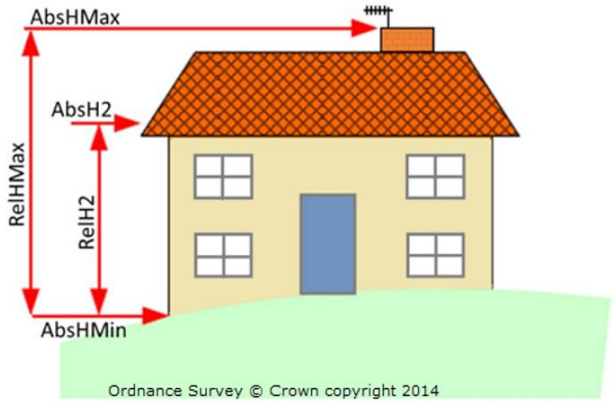

Fig. 3-Building height attributes as defined by OS.

OS publish the data as a single Comma Separated Values (CSV) file containing over 20 million records. This is a very large dataset and can cause data management problems in a desktop environment so Edinburgh Data and Information Access (EDINA) have split the

dataset up using the OS 5km grid allowing users to download the data in tiles for their study area. The data is available in CSV, Keyhole Markup Language (KML) and File Geodatabase formats.

The datasets required to generate the 3D model are:

- OS MasterMap® Topography Layer: the format selected was File Geodatabase (FileGDB) format as this format does not require any conversion to use it in Quantum Geographic Information System (QGIS), a GIS package of choice for our work which is free and open source.
- OS Terrain™ 5 DTM: this will be used as the base (surface) heights for the area;
- BHA data, selected as CSV format;
- OS VectorMap® Local Raster or 1:25 000 Scale Color Raster (used as a backdrop).

The dataset was merged in QGIS generating the 3D model displayed in Figure 4. The 3D model was exploited to generate building boundaries as described in [2] with an example of generated building boundaries illustrated in Figure 5. The boundaries are from a GNSS user's perspective, with the buildings edge determined for each azimuth (from 0 to 360°) as a series of elevation angles. The results from this step show where the building edges are located within an azimuth-elevation sky plot. Satellites are visible above this edge and blocked below it. The elevation of the building boundary is computed at a range of azimuths. Building boundaries are computed over a grid of candidate user locations. The altitude of these candidate user locations can be set at a certain distance above the ground, e.g. 1.5 m might be assumed for users holding smartphones in front of them. Only outdoor locations are considered.

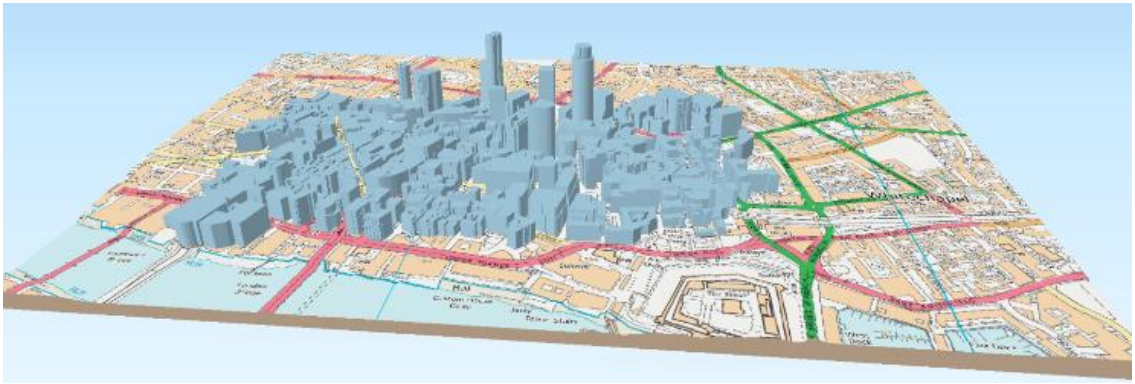

Fig. 4-OS data-derived 3D Model.

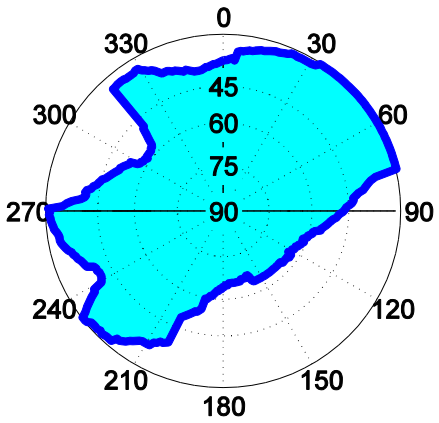

Fig. 5-Example of generated building boundaries.

Signal Selection and Weighting

With a multi-constellation GNSS receiver, the number of measurements available will normally greatly exceed the minimum number required for a position solution. Therefore, measurements contaminated by NLOS reception or multipath can be down weighted (or in some cases rejected) in order to obtain the best position solution from the measurements available. The challenge is to identify which are the best signals. In benign reception environments, this can be done using consistency checking techniques. However, this is unreliable in dense urban environments, even using a more robust algorithm. Here, we use 3D data to extend the work presented in [30] where combinations of three techniques for mitigating

the impact of NLOS and multipath interference on positioning accuracy were investigated, namely: consistency checking, elevation-based weighting and signal-strength-based weighting.

As demonstrated in [3], a position solution may be computed from a set of pseudo-range measurements using least-squares estimation. This is given by

$$\hat{\mathbf{x}}^{+} = \hat{\mathbf{x}}^{-} + \left(\mathbf{H}_G^{e\,\mathrm{T}}\mathbf{W}_\rho\mathbf{H}_G^{e}\right)^{-1}\mathbf{H}_G^{e\,\mathrm{T}}\mathbf{W}_\rho(\tilde{\mathbf{z}} - \hat{\mathbf{z}}^{-}), \quad (1)$$

where $\hat{\mathbf{x}}^{+}$is the estimated state vector, comprising the position and time solution, $\hat{\mathbf{x}}^{-}$ is the predicted state vector, $\tilde{\mathbf{z}}$ is the measurement vector, $\hat{\mathbf{z}}^{-}$ is the vector of measurements predicted from $\hat{\mathbf{x}}^{-}$, $\mathbf{W}_\rho$ is the weighting matrix and $\mathbf{H}_G^{e}$ is the measurement matrix. For GPS and GLONASS measurements with an unknown interconstellation timing offset, the state vector and measurement vector are

$$\mathbf{x} = \begin{pmatrix} \mathbf{r}_{ea}^{e} \\ \delta\rho_c^{a} \\ \delta\rho_c^{GL} \end{pmatrix} \qquad \mathbf{z} = \begin{pmatrix} \rho_{a,C}^{1} \\ \rho_{a,C}^{2} \\ \vdots \\ \rho_{a,C}^{m} \end{pmatrix}, \quad (2)$$

where $\mathbf{r}_{ea}^{e}$ is the Cartesian position, resolved about and with respect to an Earth-centred Earth-fixed (ECEF frame), $\delta\rho_c^{a}$ and $\delta\rho_c^{GL}$ are, respectively, the receiver clock offset and GLONASS-GPS timing offset, expressed as ranges, $\rho_{a,C}^{j}$ is the pseudo-range from satellite j and m is the number of satellite used. The measurement matrix is given by

$$\mathbf{H}_G^{e} = \begin{pmatrix} -u_{a1,x}^{e} & -u_{a1,y}^{e} & -u_{a1,z}^{e} & 1 & -\delta_{1\in GL} \\ -u_{a2,x}^{e} & -u_{a2,y}^{e} & -u_{a2,z}^{e} & 1 & -\delta_{2\in GL} \\ \vdots & \vdots & \vdots & \vdots & \vdots \\ -u_{am,x}^{e} & -u_{am,y}^{e} & -u_{am,z}^{e} & 1 & -\delta_{m\in GL} \end{pmatrix}, \quad (3)$$

where $\mathbf{u}_{aj}^{e}$ is the line-of-sight vector from the user antenna to satellite j and $\delta_{j\in GL}$ is 1 where satellite j is a GLONASS satellite and zero otherwise. The line-of-sight vectors and predicted pseudo-ranges, $\hat{\rho}_{a,C}^{j-}$, are given by

$$\mathbf{u}_{as}^{e} \approx \frac{\hat{\mathbf{r}}_{ej}^{e} - \hat{\mathbf{r}}_{ea}^{e-}}{\left|\hat{\mathbf{r}}_{ej}^{e} - \hat{\mathbf{r}}_{ea}^{e-}\right|}, \quad (4)$$

$$\hat{\rho}_{a,C}^{j-} = \sqrt{\left[\hat{\mathbf{r}}_{ej}^{e} - \hat{\mathbf{r}}_{ea}^{e-}\right]^{\mathrm{T}}\left[\hat{\mathbf{r}}_{ej}^{e} - \hat{\mathbf{r}}_{ea}^{e-}\right]} + \delta\hat{\rho}_{c}^{a-} + \delta_{j\in GL}\delta\hat{\rho}_{c}^{GL-} + \delta\hat{\rho}_{ie,a}^{j-}, \quad (5)$$

where $\hat{\mathbf{r}}_{ej}^{e}$ is the position of satellite j, $\hat{\mathbf{r}}_{ea}^{e-}$ is the predicted user position, $\delta\hat{\rho}_{c}^{a-}$ is the predicted receiver clock offset, $\delta\hat{\rho}_{c}^{GL-}$ is the predicted GLONASS-GPS timing offset and $\delta\hat{\rho}_{ie,a}^{j-}$ is the satellite j Sagnac correction [30].

The different weighting schemes considered are: conventional elevation-based weighting, C/N_0-based weighting and no weighting. $\mathbf{W}_\rho$ is given by

$$\mathbf{W}_\rho = \begin{pmatrix} \sigma_{\rho_1}^{-2} & 0 & \cdots & 0 \\ 0 & \sigma_{\rho_2}^{-2} & \cdots & 0 \\ \vdots & \vdots & \ddots & \vdots \\ 0 & 0 & \cdots & \sigma_{\rho_m}^{-2} \end{pmatrix}, \quad (6)$$

where, for the elevation-based weighting,

$$\sigma_{\rho j} = a + b\,\exp\left(-\theta_{nu}^{aj}/\theta_0\right), \quad (7)$$

where θ_{nu}^{aj} is the elevation angle of the j^{th} satellite and the constants are $a = 0.13\text{m}$, $b = 0.56\text{m}$ and $\theta_0 = 0.1745$ rad [32] while, for C/N_0-based weighting,

$$\sigma_{\rho j} = \sqrt{c\times 10^{-(C/N_0)_j/10}}, \quad (8)$$

where $(C/N_0)_j$ is the measured carrier-power-to-noise-density ratio of the j^{th} satellite signal in dB-Hz and $c = 1.1\times10^{4}\text{m}^2\text{s}^{-1}$ is a constant [33].

For the case without weighting, $\mathbf{W}_\rho$ is simply the identity matrix.

In this work, as indicated above, we exploit the 3D city model to classify the signals as line-of-sight (LOS) or not. As we do not know our exact position, we cannot definitively predict which signals are LOS and which are NLOS. Instead, we consider a search area of candidate positions and determine the proportion of those positions at which a direct LOS signal can be observed for each satellite. This gives us an estimate of the probability that each signal received is LOS. This additional information helps to further refine the positioning algorithm proposed in [30]. The consistency checking process, described in the next section, is modified and we

define a new weighting matrix,$\mathbf{W}_{\rho_{3D}}$, for the least-squares position solution, derived above, that incorporates this additional information. This replaces $\mathbf{W}_{\rho}$ in equation (1) and is given by

$$\mathbf{W}_{\rho_{3D}} = \begin{pmatrix} p_1\sigma_{\rho_1}^{-2} & 0 & \cdots & 0 \\ 0 & p_2\sigma_{\rho_2}^{-2} & \cdots & 0 \\ \vdots & \vdots & \ddots & \vdots \\ 0 & 0 & \cdots & p_m\sigma_{\rho_m}^{-2} \end{pmatrix}, \quad (9)$$

where the elements $p_i, i = 1, \cdots, m$, are the estimated probabilities that each signal is received via a direct LOS path.

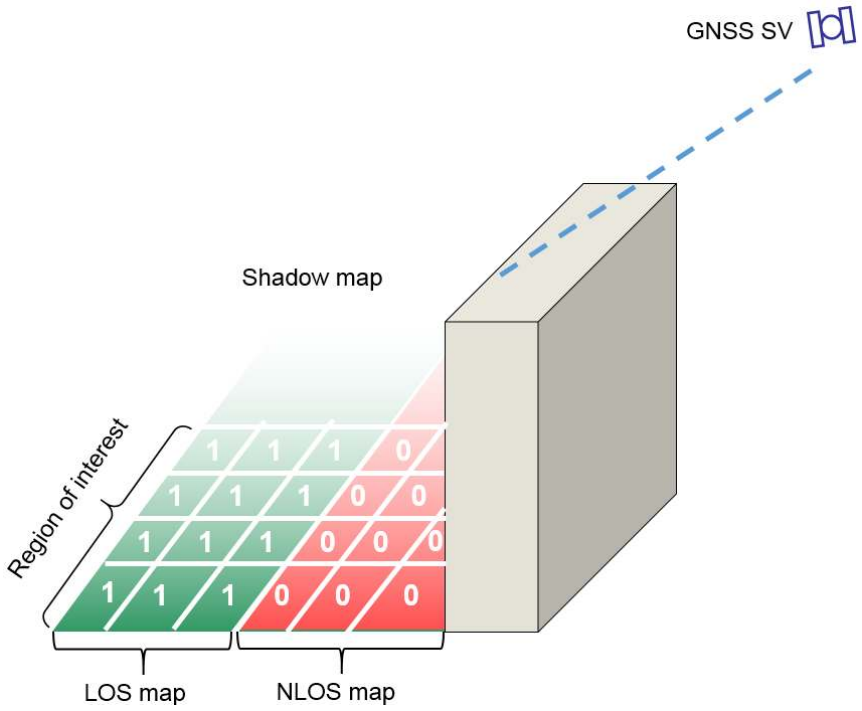

Fig. 6-Shadow map used for 3D-aided mapping weighting.

The derivation of the elements p_i is as follows: We begin by defining a circular search area with a radius between 40 and 100m. Within the search area, we define a grid of points with a meter separation and use the 3D city model to exclude those points known to be within buildings. For each satellite, we compare the azimuth and elevation with the building boundary at each grid point to determine whether the signal is direct LOS or NLOS at that point. This is equivalent to computing a shadow map from a city building map (within the region of interest) with respect to a GNSS satellite position by projecting the buildings onto the surface, as

illustrated by Figure 6. The direct LOS map of each considered signal is represented as a 2D matrix filled with the elements "1" or "0", each indicating whether or not the receiver has a direct LOS to the corresponding GNSS satellite at that grid point (similarly, an NLOS map could be generated by switching the 1 and 0 values). By calculating a simple average of the "1"s and "0"s across all outdoor locations within the search area, we determine a LOS probability p_i for each satellite. The overall likelihood weightings are then determined by multiplying the LOS probabilities with the C/N_0 -derived or elevation-based weighting factors, $\sigma_{\rho_i}^{-2}$, described previously. In this work, the considered shadow map region is a square centered at the conventional GNSS position solution with a side of 200m.

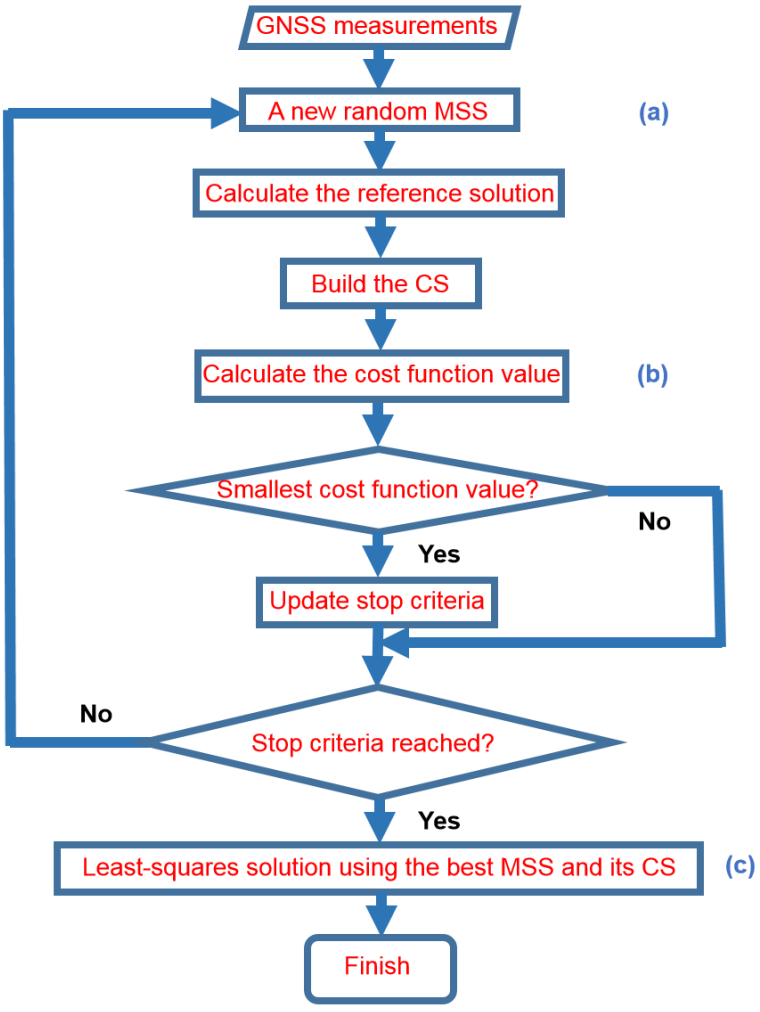

Fig. 7-Approach to positioning using consistency checking proposed in [30].

Consistency Checking

We recall that the consistency checking technique presented in [30], and illustrated in Figure 7, looks at identifying the subset of GNSS measurements and height-aiding virtual range (referred thereafter as GNSS plus height-aiding measurements) that are most consistent with each other (the height-aiding process is explained in the next sub-section). The subset comparison method works by scoring different subsets of the GNSS plus height-aiding measurements according to their consistency and then using the most consistent subset to form the position solution. The basis of this method is the Minimal Sample Set (MSS), where a subset solution is only selected in preference to the all-signal solution when a highly consistent subset is available. Each MSS is used to predict the remaining pseudo-ranges, which are compared with their measured values, both to score the MSS and to identify which of the measurements are consistent with it. The algorithm considered is based on a technique known as Random Sample Consensus (RANSAC), which uses random-draw subsets of the measurements and a probability-based stopping criterion for efficiency. The MSS is then assessed, resulting in a Consensus Set (CS) and a cost function which is a measure of consistency. The CS is the set of measurements outside the MSS that are found to be consistent with the MSS, defined as the magnitude of the residual, e_j^i, being within a pre-defined threshold, δ. The cost function C^i, corresponding to the i^{th} MSS, is defined by (assuming a Gaussian distribution).

$$C^i(\mathbf{e}^i) = \sum_{j=1}^{m} k(e_j^i, \delta), \qquad (10)$$

where

$$k(e_j^i, \delta) = \begin{cases} |e_j^i|/\sigma_{\rho j} & |e_j^i| \le \delta \\ \delta/\sigma_{\rho j} & |e_j^i| > \delta \end{cases}, \qquad (11)$$

where $\sigma_{\rho j}$ are given by (7) and (8) and e_j^i are the elements of vector $\mathbf{e}^i$. This latter is calculated using

$$\mathbf{e}^i = \tilde{\mathbf{z}} - \hat{\mathbf{z}}^{+i}, \qquad (12)$$

where $\hat{\mathbf{z}}^{+i}$ is the set of measurements predicted from the i^{th} MSS position and time solution, $\hat{\mathbf{x}}^{+i}$, given by

$$\hat{\mathbf{x}}^{+i} = \hat{\mathbf{x}}^{-} + \mathbf{H}_G^{e,i^{-1}}\left(\mathbf{z}^{\boldsymbol{i}} - \hat{\mathbf{z}}^{i-}\right). \qquad (13)$$

Where $\mathbf{H}_G^{e,i}$ comprises the rows of the measurement matrix, $\mathbf{H}_G^e$, given by (3), which correspond to the i^{th} MSS, $\hat{\mathbf{z}}^{i-}$ comprises the elements of the predicted measurement vector, $\hat{\mathbf{z}}^{-}$, given by (2), corresponding to the i^{th} MSS and $\hat{\mathbf{x}}^{-}$is the predicted state vector, also defined by (2).

The process is iterated to find a MSS that generates the minimum cost function. This continues until there have been sufficient iterations for the probability of finding a better MSS to fall below a certain threshold [30]. In cases where the MSS with the lowest cost function has no measurements in its consensus set, it is not possible to confirm that this measurement subset (or any other) is self-consistent, so consistency checking is deemed to have failed and the all-satellite position solution is used.

In our new approach exploiting the 3D city model, the MSS generation step, indicated by (a) in Figure 7, is modified as follows: The samples, unlike in [30], are not drawn from all measurements, but from a subset of the data with the highest quality (i.e. the measurements with the highest p_i). We further explain the difference between our approach and the one proposed in [30] using the following example: Imagine the algorithm in [30] drawing T_N samples of size m out of N measurements. Let $\{M_i\}_{i=1}^{T_N}$denote the sequence of samples $M_i \subset U_N$ (where $U_N$is the set of all tentative correspondences) that are uniformly drawn by [30], and let $\{M_{(i)}\}_{i=1}^{T_N}$ be sequence of the same samples sorted in descending order according

to the sample quality: $i < j \Rightarrow q\left(M_{(i)}\right) \geq q\left(M_{(j)}\right)$ (where q is a quality function, in our case corresponding to p_i). If the samples are taken in order $M_{(i)}$, the samples that are more likely to be uncontaminated are drawn earlier. Progressively samples containing data points with lower quality function are drawn.

Furthermore, an additional weighting is applied to the cost function indicated in Figure 7 as (b) and used to derive the consensus set (CS). This results in a modified cost function, C_{3D}^{i}, given by

$$C_{3D}^{i}\left(\mathbf{e}^{i}\right) = \sum_{j=1}^{m} k_{3D}\left(e_j^i, \delta\right), \qquad (14)$$

where

$$k_{3D}\left(e_j^i, \delta\right) = \begin{cases} p_j \left|e_j^i\right| / \sigma_{\rho j} & \left|e_j^i\right| \leq \delta \\ p_j \delta / \sigma_{\rho j} & \left|e_j^i\right| > \delta \end{cases}. \qquad (15)$$

Terrain Height-Aiding

Many conventional maps, dedicated digital terrain models (DTMs) and digital elevation models (DEMs) and all 3D maps provide the terrain height. Land vehicle or pedestrian GNSS user equipment may be assumed to be at a fixed height above the terrain. Therefore, the approximate GNSS horizontal position solution may be used to obtain a height solution from the mapping data or a separate terrain height database. This may then be used as an extra ranging measurement within a GNSS positioning algorithm, a technique known as height-aiding [28]. Typically, the height-aiding measurement is treated as a virtual transmitter at the center of the Earth, the range to which is equal to the (local) Earth radius plus the height (Figure 8).

If the terrain within the search area is not flat, the range may vary over the uncertainty bounds of the approximate GNSS position solution. Therefore, for best accuracy, computation of the

position solution and height-aiding measurement should be iterated until convergence is achieved.

Height-aiding is particularly useful in cases where there are insufficient direct-LOS signals to determine a position solution without using NLOS signals. Under good GNSS reception conditions, height-aiding only improves vertical positioning. However preliminary tests using simulated height [30] have shown that in areas such as urban canyons, where the signal geometry is poor, it can also improve horizontal positioning.

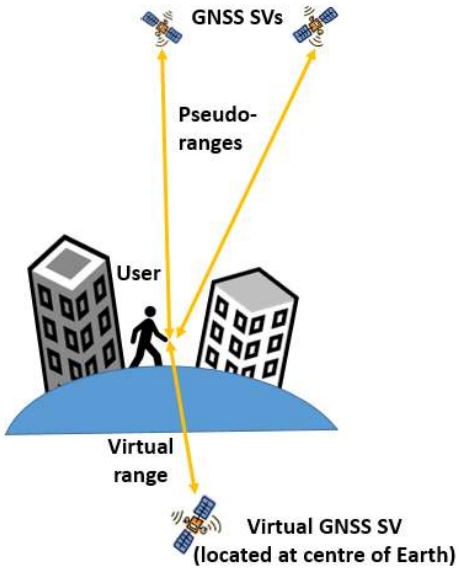

Fig. 8-Terrain height-aiding.

Considering m GNSS range measurements, the height-aiding measurement forms the $m + 1^{th}$ component of the measurement vector, $\boldsymbol{z}$, defined in (2). The height-aiding row of the measurement matrix is [30].

$$\mathbf{H}^{e}_{G,m+1} = (u^{e}_{ea,x} \quad u^{e}_{ea,y} \quad u^{e}_{ea,z} \quad 0 \quad 0), \quad (16)$$

where $\mathbf{u}^{e}_{ea}$is the unit vector describing the direction from the center of the Earth to the predicted user position, given by

$$\mathbf{u}_{ea}^{e} \approx \frac{\hat{\mathbf{r}}_{ea}^{e-}}{|\hat{\mathbf{r}}_{ea}^{e-}|}, \qquad (17)$$

and the state vector is as defined in (2). Here we generate height-aiding measurements using a terrain height database and the unaided GNSS position solution. A constant weighting coefficient for the virtual height-aiding range measurement was used. Its value was determined empirically. The weighting strategy for the actual GNSS pseudorange measurements, based on satellite elevation, C/N_0 ratio, LOS probability and shadow map probabilities, does not apply to the virtual range. It equals to the inverse of the variance assumed on the pseudo-measurement (in this` case, the virtual range).

Figure 9 summarizes the iterative process of computing height-aiding comprising three main steps:

1. A position is computed using pseudo-range measurements from all of the satellites tracked as described in equation (1) (using one of the weighting strategies described in Signal Selection and Weighting sub-section).
2. Following the computed position and coordinate transformation from WGS84 to the National Grid Easting and Northing coordinate system, a database containing terrain height information is then queried and the four DTM vertices surrounding the position solution are identified and extracted. These latter are then used in an interpolation process (as described in the next paragraphs) to extract a new height corresponding to the computed position.
3. Following conversion of the height to a virtual range measurement, this is then added to the measurement vector and a new position solution is computed. The process is iterated until the difference between the old and new position is smaller than the DTM cell resolution.

We examined the effect of different terrain resolutions, obtained from Ordnance Survey (OS) grid DTM 5 and DTM 50 (with 5m and 50m grid resolution, respectively, and both

having a 1.5m height resolution) [31], on horizontal position and height accuracy for urban mobile positioning. The choice of interpolation algorithm for estimating heights from the DTM was also investigated.

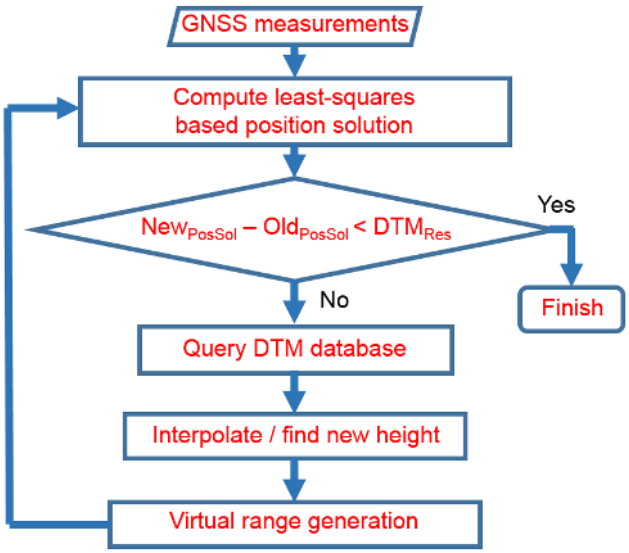

Fig. 9-Terrain Height-Aiding Process.

GNSS position solutions are unlikely to correspond to the grid points in any DTM. Therefore heights for aiding GNSS positioning must be interpolated from surrounding points in the DTM. There are a variety of interpolation algorithms [34] (e.g. linear, bilinear, bicubic and biquintic). A higher order interpolant that takes account of the points beyond those immediately surrounding the position of interest, either directly or indirectly as slope estimates, will generally produce a better estimate than the bilinear algorithm. However, the more complex an interpolation algorithm is, the more computationally expensive it becomes, which may be a prohibitive overhead when computing GNSS positions using consumer devices such as smartphones. The first part of the work described here investigates how the choice of DTM and interpolation method affects the performance of the proposed positioning algorithm, in terms of horizontal position and height accuracy.

The study reported in [34] demonstrates that whether interpolating on mathematical surfaces or DTMs, irrespective of terrain complexity, the higher-order algorithms consistently

outperform the simpler linear variant. For this study, two representative high-order interpolation algorithms, bicubic and biquintic, were tested, as well as the more popular bilinear algorithm, often incorporated in desktop Geographic Information System (GIS) packages. Bicubic interpolation gave significant better positioning performance than bilinear interpolation but the performance of bicubic and biquintic interpolation was similar [35]. Therefore, bicubic interpolation has been selected.

The most commonly used interpolation method for a regular grid is patchwise polynomial interpolation. The general form of this equation for surface representation is [34]

$$h(x,y) = \sum_{i=0}^{m}\sum_{j=0}^{n} a_{ij}x^i y^j , \qquad (18)$$

where $h(x,y)$ is the height of an individual point with rectangular coordinates x and y, and $\{a_{ij}, i = 0,\cdots,m, j = 0,\cdots,n\}$ are the coefficients of the polynomial in (18).

Bicubic interpolations makes use of a 16-term function can be represented by (18) with $m = n = 3$. Since the coordinates of each grid vertex are known, the values of $\{a_{ij}, i = 0,\cdots,3, j = 0,\cdots,3\}$ can be determined from a set of simultaneous equations based on (18), one for each known point, or its derivative. Having determined the coefficients, a_{ij}, the height for a location with known horizontal coordinates can be determined using (18).

In order to solve the 16 coefficients, the heights at the four vertices of the grid cell, together with three derivatives (in total 16 values) are calculated. The first derivatives with respect to x and y, $\partial_x h(x,y)$ and $\partial_y h(x,y)$, express the slope of the surface in the x and y directions, respectively, whilst the second-order cross derivative, $\partial_{xy} h(x,y)$, represents the slope in both x and y. For the bicubic interpolation it is necessary to estimate the derivatives or slopes at the DTM vertices. Slope values will influence the shape of the interpolating surface function in a more valuable and accurate way than just using additional DTM vertices [36]. To estimate

these slopes from the grid heights, we used finite difference approximations [37] where the different slopes are calculated as follows:

$$\partial_x h(x_i, y_i) = \frac{h(x_{i+1}, y_i) - h(x_{i-1}, y_i)}{2(x_{i+1} - x_{i-1})}$$

$$\partial_y h(x_i, y_i) = \frac{h(x_i, y_{i+1}) - h(x_i, y_{i-1})}{2(y_{i+1} - y_{i-1})}$$

$$\partial_{xy} h(x_i, y_i) \tag{19}$$

$$= \frac{h(x_{i+1}, y_{i+1}) - h(x_{i-1}, y_{i+1}) - h(x_{i+1}, y_{i-1}) + h(x_{i-1}, y_{i-1})}{4(x_{i+1} - x_{i-1})(y_{i+1} - y_{i-1})}$$

Initialization Process

The approach proposed in this work relies on the definition of a search area around the unknown actual position. This is done by considering the conventional GNSS solution as the center of a circle with a pre-defined radius (a typical 40m radius was considered based on the work performed in [24]). Relying on the conventional GNSS solution as a basis for the selection of the search area is not a robust approach especially in a deep urban environment where the conventional GNSS solution might be more than 40m away from the true position. Here, we propose two iterative initialization approaches. A single-stage process is described first, followed by a two-stage process.

The single-stage initialization approach is illustrated in Figure 10. The idea is to take the conventional GNSS receiver position solution and consider a large search area, larger than the typical 40m search radius considered before (in our work we have selected an initial search radius of 100m with a grid spacing of 15m). We then apply the height-aiding and 3D-city-model aided signal selection and weighting, using the height averaged across the search area and extracted from the 3D city model. The resulting position solution is then considered as the center of a new search area with a reduced search radius (in our work we reduced the search

radius with decrements of 20m) with the new height still averaged across the search area and a reduced grid spacing (in this work we reduced the grid spacing by decrements of 3 meters).

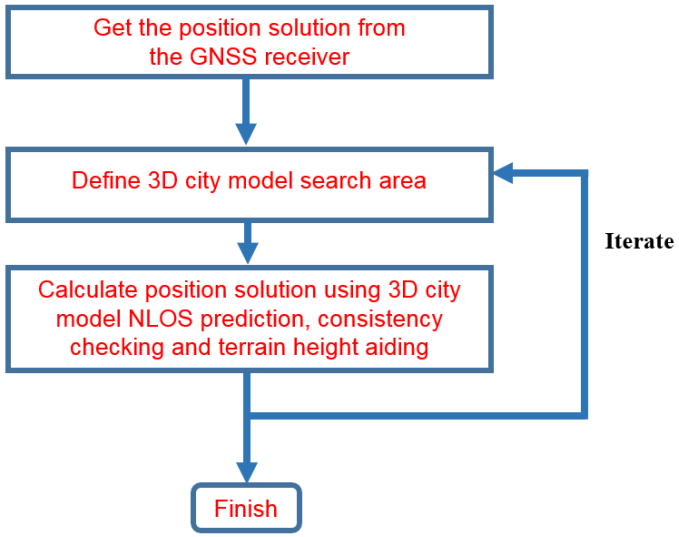

Fig. 10- Proposed approach with single-stage initialization.

The process is iterated until we reach a search area radius of 40m. Following the completion of the initialization process, a height-aiding (considering the actual height at each search area point and extracted from the 3D city model as opposite to the previously averaged height across the search area) and 3D-city-model aided signal selection and weighting is performed considering the position solution outputted by the initialization stage as the center of a search area of 40m radius and 1m grid spacing.

If the true position is outside of the search area, the wrong region of the 3D city model is used for NLOS prediction. This can result in the NLOS prediction adversely affecting the performance of the consistency checking process.

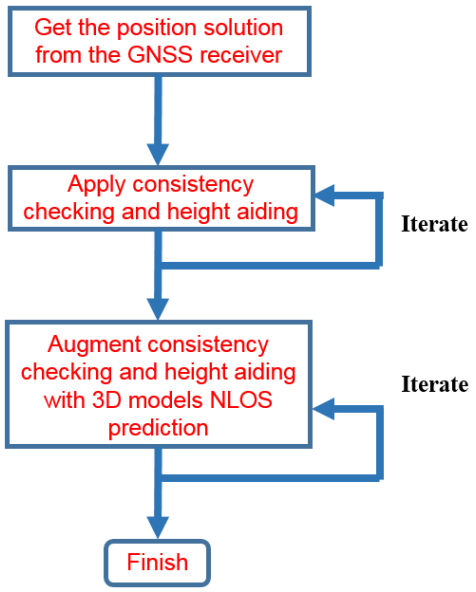

Fig. 11-Proposed approach with two-stage initialization.

The initialization strategy shown in Figure 11 solves this problem through a two stage iteration process. The first stage applies height-aiding and consistency checking process on the conventional GNSS without employing the 3D model-based weighting. The average height across the search area is considered for this stage. The second stage then proceeds as shown in Figure 10, making use of NLOS predictions from the 3D model. A 60m search radius was considered at the beginning of this second stage this to accommodate for the originally very poor conventional GNSS horizontal accuracy and taking into account the expected improvement in horizontal accuracy using the consistency checking and height-aiding [35].

EXPERIMENTAL RESULTS

The combined height-aiding and 3D model-based NLOS prediction algorithm was tested using GPS and GLONASS data collected using a Leica Viva GS15 survey-grade multi-constellation GNSS receiver in Central London (test sets 1 and 2) and using a u-blox evaluation kit (EVK-M8T), which is a multiconstellation GNSS receiver (GPS/GLONASS and Galileo ready) [38] (Test Set 3). The first set of test data was collected near Moorgate underground station on 8th April 2011. There are three sites within the test data set, each occupied for about

38 minutes. The truth was established using traditional surveying methods and is accurate at the cm-level.

The second test data set was collected near Fenchurch Street station on 23rd July 2012. Overall, 22 sites were occupied to cover a variety of environments. Each site was occupied for two periods of about 10 minutes approximately 3 hours apart. The truth was established to decimeter-level accuracy using a 3D city model with tape measurements from landmarks. Figure 12 shows an overview of the test sites.

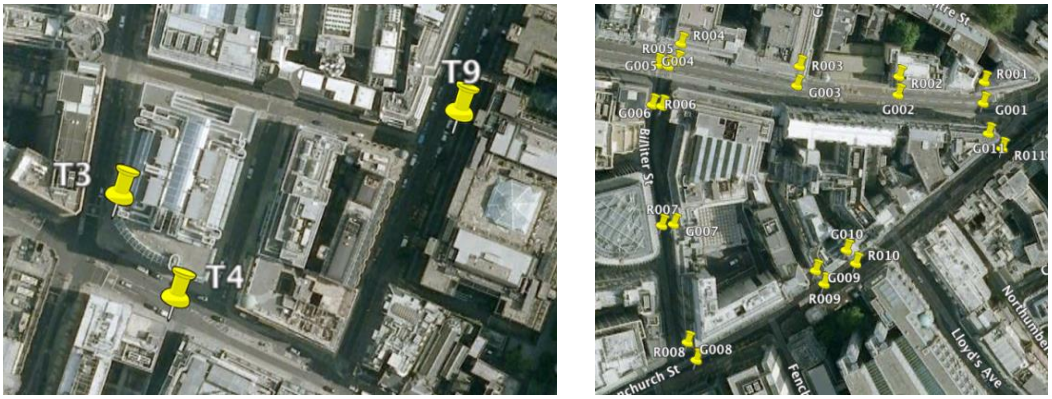

Fig. 12-Locations of the test set 1 (left) and test set 2 sites (right) (Background Image © 2013 Bluesky © Google).

To validate the estimation of LOS probability using the city model, we analyzed the estimated LOS probability for all LOS and NLOS signals at all epochs and across all sites. This was done by first working out which signals are really LOS and NLOS at each site and epoch (using the true location and building boundaries). This enables the classification of the LOS probabilities (referred to in the manuscript as p_i). Figure 13 presents a histogram plot of the two set of p_i (for LOS and NLOS signals). We can see from the figure that the majority of LOS signals have a value of p_i over 50% and most NLOS signals have a value of p_i lower than 50%. Therefore, comparing the proportion of the proportion of the search area over which each signal is

predicted by the 3D city model to be LOS is an effective way of estimating the likelihood that a signal is LOS or NLOS.

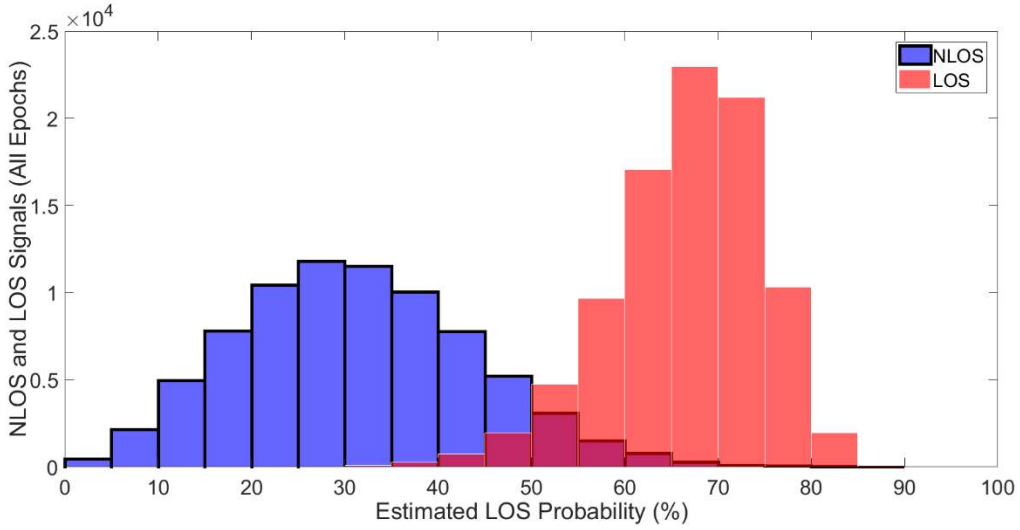

Fig. 13-Estimated LOS probability for NLOS and LOS signals at all epochs across all sites.

We analyzed the impact of varying the assumed standard deviation of the height-aiding measurements with the least-squares weight matrix, between 0.1m and 10m, in order to identify the optimum value (in terms of horizontal positioning performance, in RMS). Separate optimizations were performed: for the approach with height-aiding only and for the approach including height-aiding and 3D model-aiding. A value of 0.9m was found for the former and of 1.6m for the latter. Thus, a lower weighting for the height-aiding measurement works better when LOS/NLOS predictions from the 3D city model are used.

Height-aiding and consistency checking without 3D model-based NLOS prediction was tested using a number of different algorithm configurations. These results are given in Table 1 summarizing the RMS horizontal and vertical position error with conventional GNSS positioning and terrain height-aiding for both C/N_0 and elevation based weighting and using OS DTM 5 and DTM 50.

Table 1 - Position errors – Height-aiding only approach and average RMS error for test sets 1 and 2 using different combinations.

Positioning			Average RMS Positioning Error (m)	
Terrain Aiding		Weighting	Horizontal	Vertical
None		Elevation	50.1	53.9
		(C/N_0)	46.1	50.1
Bicubic interpolation and a 5m/50m grid spacing	DTM 50	Elevation	34.7	11.8
		(C/N_0)	31.5	13.1
	DTM 5	Elevation	29.8	9.9
		(C/N_0)	25.9	10.3

The terrain-aiding results presented are those using the bicubic polynomial as it provided similar results to the biquintic polynomial interpolation and better overall performance than a bilinear interpolant [35]. This configuration is used for all subsequent results in the paper. With C/N_0-based weighting, terrain height-aiding improved the horizontal accuracy by 44% with DTM 5 and 32% with DTM 50.

We have tested the height-aiding approach augmented with the 3D aided signal selection at all sites. Figure 14 illustrates the achieved improvements in positioning at location T9. The RMS horizontal position error was reduced by 64% and the vertical error by 83%. Table 2 summarizes the results at all locations within test sets 1 and 2.

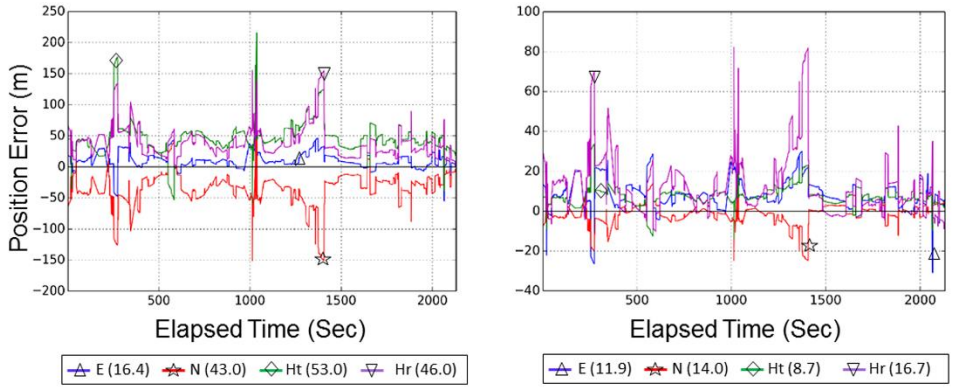

Fig. 14-Position error, location T9 - conventional GNSS positioning (left) and The 3D model-based NLOS prediction and height-aiding approach. The figures in the legend are RMS errors in meters (*the markers are used to distinguish the different plots for black and white prints and are not corresponding to the RMS error values reported on the legend. This also applies to Figure 17, 18, 19 and 20*).

Table 2 - Average position errors obtained using terrain height-aiding and 3D model-based NLOS prediction – Test sets 1 and 2

Positioning Algorithm	Average RMS Positioning Error (m)	
	Horizontal	Vertical
Conventional GNSS (using C/N_0 weighting)	46.1	50.1
Terrain Height-aiding only (DTM5 and (C/N_0) weighting)	25.9	10.3
Terrain Height-aiding and 3D model-based NLOS Prediction	20.1	9.0
Accuracy Improvement	56%	82%

A third dataset was collected near Fenchurch Street station on the 15th of May 2015 using u-blox EVK-M8T GNSS receiver; the 4 selected sites are illustrated in Figure 15 and in Figure 16. The truth was established to decimeter-level accuracy using a 3D city model with tape measurements from landmarks.

We have evaluated the combined 3D aided signal selection and height-aiding approach using this data. Figure 17, Figure 18 and Figure 19 illustrate the positioning error using conventional GNSS positioning (with consistency checking and C/N_0 weighting), height-aiding, and the new approach (height-aiding and 3D model-based NLOS prediction aiding, with the single-stage initialization), respectively. Table 3 summarizes the improvement in position accuracy

for each location. Note that conventional positioning at site S4 is 40% poorer than at the other sites. Using the new method, the RMS position error across all four sites was 21.6m horizontally and 15.4m vertically.

Fig. 15-Locations of the Test Set 3 sites (Background Image © 2015 Bluesky © Google).

Fig. 16-Locations and skylines for Test Set 3.

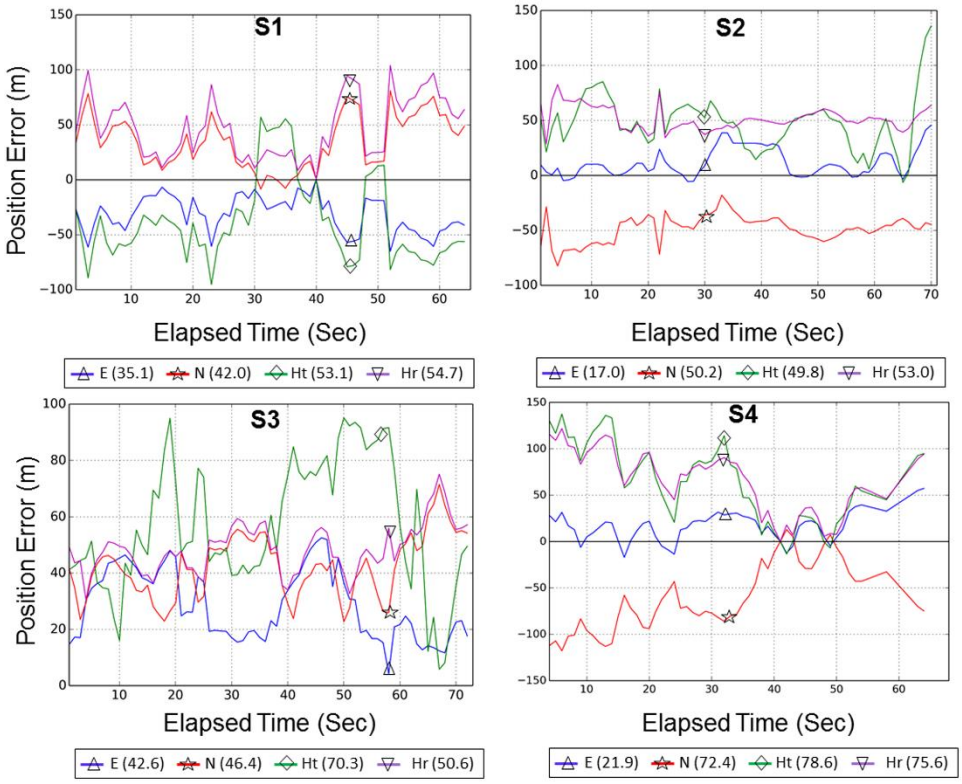

Fig. 17-Position error using conventional GNSS positioning – u-blox data collected at Test Set 3. The figures in the legends are RMS errors in meters.

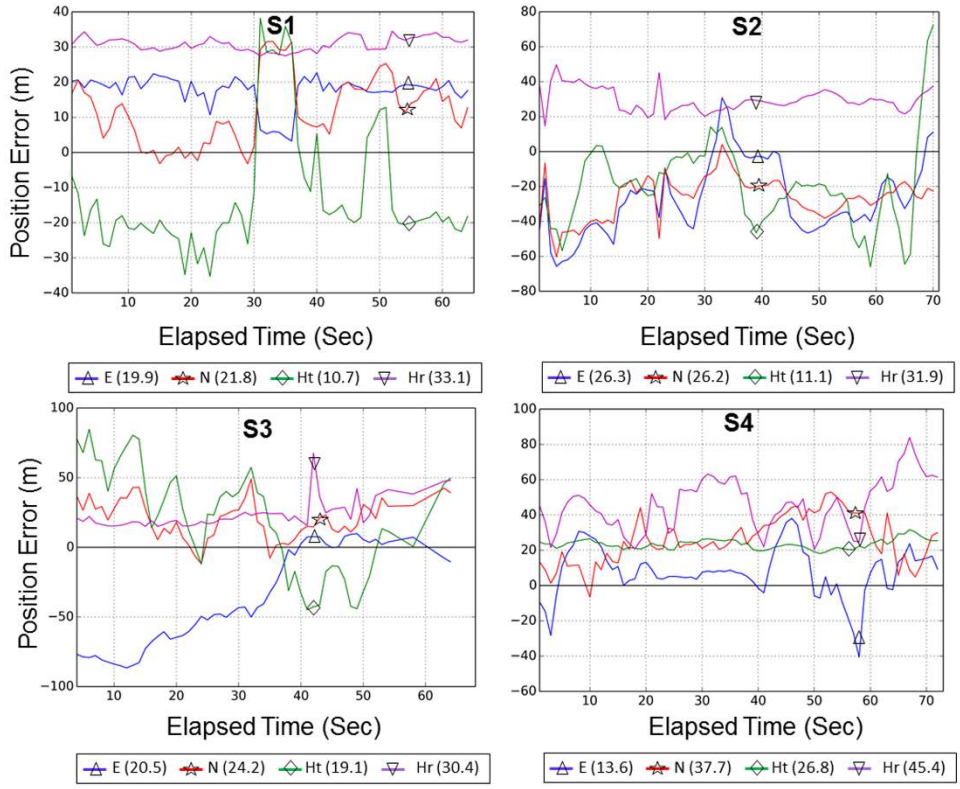

Fig. 18-Position error using height-aiding approach – u-blox data collected at Test Set 3. The figures in the legends are RMS errors in meters.

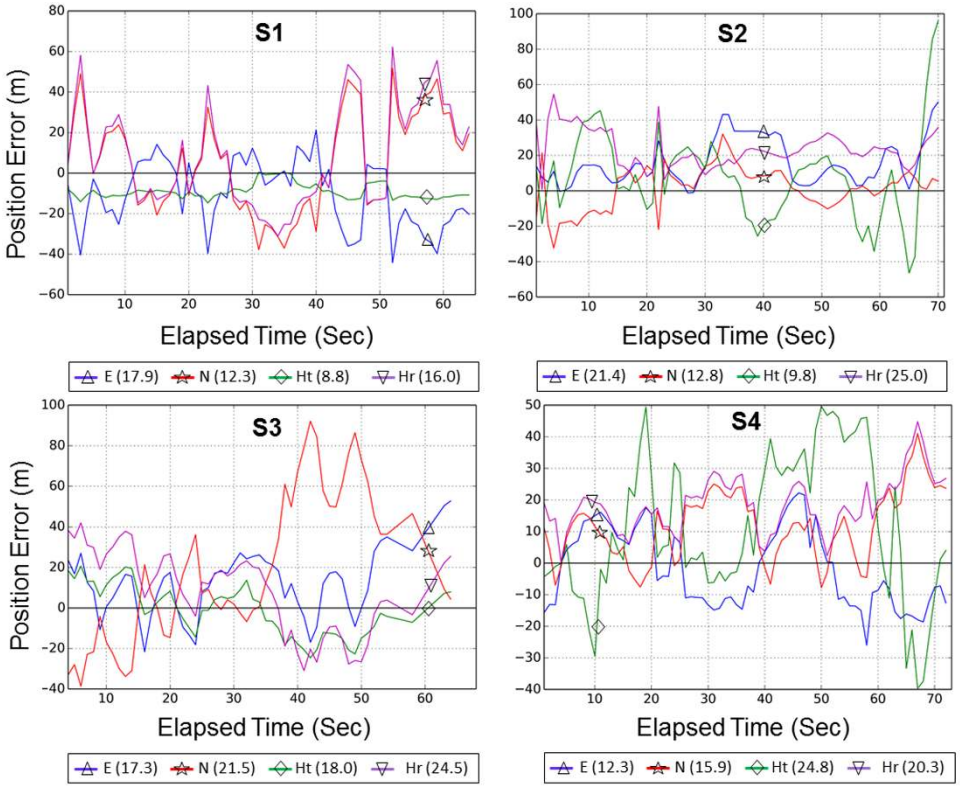

Fig. 19-Position error using the 3D model-based NLOS prediction and height-aiding approach – u-blox data collected at Test Set 3. The figures in the legends are RMS errors in meters.

Table 3 - Position accuracy improvement using terrain height-aiding and 3D model-based NLOS prediction (compared to conventional GNSS positioning with consistency checking) – Locations S1, S2, S3, and S4 on Figure 15.

Approach	Location	Improvement in Accuracy	
		Horizontal	Vertical
Height-aiding only	S1	38%	79%
	S2	37%	78%
	S3	39%	73%
	S4	40%	66%
	All	38%	74%
Height-aiding augmented with the 3D aided signal selection	S1	71%	83%
	S2	53%	80%
	S3	52%	74%
	S4	73%	69%
	All	62%	77%

Further data was collected at site S2 where it was found that the conventional GNSS solution used to initialize the new approach was more than 163m away from the true position. This makes it a good candidate to test our second initialization technique illustrated in Figure 11.

The results obtained using single-stage and two-stage initialization approaches are illustrated in Figure 20. It is clear that the two-stage initialization approach resolved the problem of the initial position error being too large for the single-stage initialization approach to handle (Where the single-stage initialization approach resulted in a larger error compared to the GNSS receiver calculated solution).

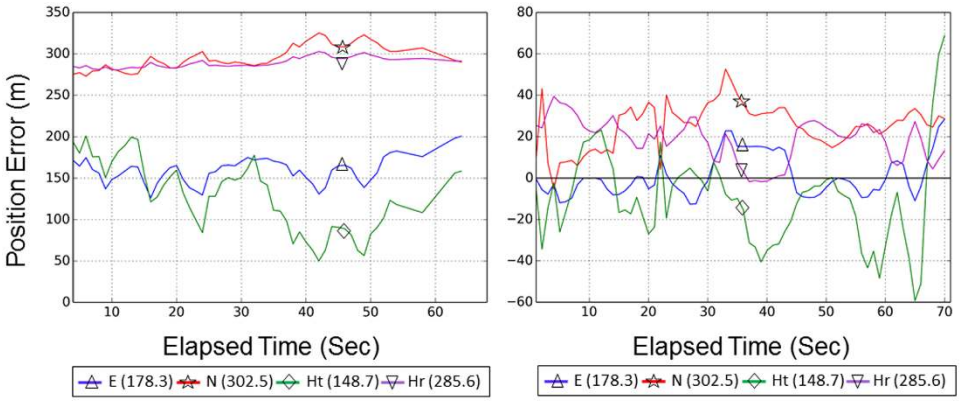

Fig. 20-3D model-based NLOS prediction and height-aiding with the single-stage initialization approach (left) and two-stage initialization approach (right). The figures in the legends are RMS errors in meters.

At all of the other test sites (26 location displayed on Figure 12 and Figure 15), the positioning performance using the two initialization techniques was almost the same. The mean difference in RMS horizontal and vertical position error across all test sites between the two methods was 0.7m and 1.1m, respectively.

CONCLUSIONS AND FURTHER WORK

The ability of height-aiding to improve GNSS positioning in dense urban areas using an iterative process has been assessed using data collected at multiple sites. Using a height-aiding measurement from a 3D city model or separate terrain height database significantly improves

the single-epoch positioning accuracy, horizontally as well as vertically, due to the improved solution geometry. Using Leica Viva geodetic receiver measurements and comparing to the conventional GNSS positioning using C/N_0 weighting, horizontal accuracy is improved by 44% and vertical accuracy by 79%.

Augmenting the height-aiding with 3D city model-based NLOS prediction aids signal selection and weighting using consistency checking further improved the accuracy by 22% horizontally and 13% vertically. The combined improvement was 56% horizontally and 82% vertically, a factor of 2.3 and 5.5, respectively. A u-blox EVK-M8T consumer-grade receiver was also used with the height-aiding and the 3D model-based NLOS prediction and the overall accuracy improvement across four locations in a dense urban area was of 62% horizontally and 77% vertically, a factor of 2.7 and 4.1, respectively. The overall improvement, considering the data collected from both receivers, was 61% horizontally and 80% vertically, a factor of 2.5 and 5, respectively. The overall RMS position error using the new method was 20.8m horizontally and 12.2m vertically.

Iterative initialization strategies have been demonstrated that accommodate the fact that the receiver does not possess an accurate knowledge of the actual position. It was found that using only height-aiding in the initial iterations, with 3D city model-based NLOS prediction introduced in later iterations, performance was better when the conventional GNSS horizontal error exceeded 100m.

In future work we plan to integrate the techniques presented here with GNSS shadow matching [24], a concept known as intelligent urban positioning [8]. We also propose to develop a more sophisticated ranging-based GNSS positioning algorithm that uses NLOS prediction from the 3D city model at individual candidate position instead of the average NLOS position across the search area. This will also be integrated with shadow matching. The algorithms presented here will then be used for initialization, minimizing the search area for

the subsequent positioning algorithms. Applications that could benefit from this include vehicle lane detection for intelligent transportation systems (ITS), location-based advertising, augmented-reality, and step-by-step guidance for the visually impaired and for tourists.

ACKNOWLEDGEMENTS

This work is funded by the Engineering and Physical Sciences Research Council (EPSRC) project EP/L018446/1, Intelligent Positioning in Cities using GNSS and Enhanced 3D Mapping. The project is also supported by Ordnance Survey, u-blox and the Royal National Institute for Blind People.

The paper exploits some data collected in 2011-12 by Dr Zyi Jiang under EPSRC project EP/G019622/1, Extending the Applications and Improving the Efficiency of Positioning Through the Exploitation of New GNSS Signals.

REFERENCES

[1] Ballester-Gúrpide, Í., et al. (2000). Future GNSS Constellation Performances Inside Urban Environments, Proceedings of ION GPS 2000, Salt Lake City, Utah.

[2] Wang, L., Groves, P., Ziebart, M. (2012). Multi-Constellation GNSS Performance Evaluation for Urban Canyons Using Large Virtual Reality City Models, Journal of Navigation, 65, 459–476. Also available from http://discovery.ucl.ac.uk/.

[3] Groves, P. D. (2013). Principles of GNSS, Inertial, and Multisensor Integrated Navigation Systems, 2nd Ed., Artech House, Boston|London.

[4] Groves, P. D.,Wang, L., Walter, D., Martin, H., Voutsis, K., Jiang, Z. (2014). The Four Key Challenges of Advanced Multisensor Navigation and Positioning, IEEE/ION PLANS 2014. Monterey, California. Also available from http://discovery.ucl.ac.uk/.

[5] Groves, P. D. (2014). The Complexity Problem in Future Multisensor Navigation and Positioning Systems: A Modular Solution, Journal of Navigation, Vol. 67, pp. 311−206. Also available from http://discovery.ucl.ac.uk/.

[6] Groves, P.D., H. Martin, K. Voutsis, D. Walter, and L. Wang. (2013). Context Detection, Categorization and Connectivity for Advanced Adaptive Integrated Navigation, Proceedings of ION GNSS+ 2013, Nashville, Tennessee. Also available from http://discovery.ucl.ac.uk/.

[7] Walter, D. J., Groves, P. D., Mason, R. J., Harrison, J., Woodward, J. and Wright, P. (2015). Road Navigation Using Multiple Dissimilar Environmental Features to Bridge GNSS Outages, Proceedings ION GNSS+ 2015, Tampa, Florida. Also available from http://discovery.ucl.ac.uk/.

[8] Groves, P. D., Z. Jiang, L. Wang, and M. K. Ziebart. (2012). Intelligent Urban Positioning using Multi-Constellation GNSS with 3D Mapping and NLOS Signal Detection, Proceedings of ION GNSS, Nashville, Tennessee. Also available from http://discovery.ucl.ac.uk/.

[9] Jiang Z., Groves P. D. (2014). NLOS GPS signal detection using a dual-polarisation antenna, GPS Solutions, 18(1):15-26. doi: 10.1007/s10291-012-0305-5. Also available from http://discovery.ucl.ac.uk/.

[10] Groves, P. D. and Jiang. Z. (2013). Height Aiding, C/N0 Weighting and Consistency Checking for GNSS NLOS and Multipath Mitigation in Urban Areas, Journal of Navigation, 66, 2013, 653−669. Also available from http://discovery.ucl.ac.uk/.

[11] Quddus, M. A., Ochieng, W. Y., and Noland, R. B. (2007). Current Map-Matching Algorithms for Transport Applications: State-of-the-art and Future Research Directions, Transportation Research Part C, 15(5), 312−328.

[12] Obst, M., et al. (2012). Urban Multipath Detection and mitigation with Dynamic 3D Maps for Reliable Land Vehicle Localization, IEEE/ION PLANS 2012.

[13] Peyraud, S., et al. (2013). About Non-Line-Of-Sight Satellite Detection and Exclusion in a 3D Map-Aided Localization Algorithm, Sensors, 13, pp. 829-847.

[14] Bourdeau, A., Sahmoudi, M., and Tourneret, J.-Y. (2013). Prediction of GNSS Signal Bias Using a 3D Model in Urban Environments, European Navigation Conference 2013, Austria.

[15] Suzuki, T., and Kubo N. (2013). Correcting GNSS Multipath Errors Using a 3D Surface Model and Particle Filter, Proceedings ION GNSS+ 2013, Nashville, Tennessee.

[16] Kumar, R. and Petovello, M, G. (2014). A Novel GNSS Positioning Technique for Improved Accuracy in Urban Canyon Scenarios using 3D City Model, Proceedings of ION GNSS+ 2014, Tampa, Florida.

[17] Hsu, L.-T., Gu, Y., and Kamijo, S. (2015). 3D building model-based pedestrian positioning method using GPS/GLONASS/QZSS and its reliability calculation, *GPS Solutions*, Vol. 20, pp. 413-428, doi 10.1007/s10291-015-0451-7.

[18] Hsu, L.-T., Gu, Y., and Kamijo, S. (2015). NLOS Exclusion using Consistency Check and City Building Model in Deep Urban Canyons, Proceedings Of ION GNSS+ 2015, Tampa, Florida.

[19] Betaille, D., et al. (2013). A New Modeling Based on Urban Trenches to Improve GNSS Positioning Quality of Service in Cities, *IEEE Intelligent Transportation Systems Magazine*, 5(3), 59–70.

[20] Groves, P. D. (2011). Shadow Matching: A New GNSS Positioning Technique for Urban Canyons. Journal of Navigation, 64, 417-430. Also available from http://discovery.ucl.ac.uk/.

[21] Wang, L., Groves, P. D. and Ziebart, M. K. (2013). GNSS Shadow Matching: Improving Urban Positioning Accuracy Using a 3D City Model with Optimized Visibility Prediction Scoring. NAVIGATION, 60, 195–207. (First published at ION GNSS 2012). Also available from http://discovery.ucl.ac.uk/.

[22] Yozevitch, R., Ben-Moshe, B. & Dvir, A. (2014). GNSS Accuracy Improvement Using Rapid Shadow Transitions. IEEE Transactions on Intelligent Transportation Systems, PP (99), 1-10.

[23] Isaacs, J. T., et al. (2014). Bayesian localization and mapping using GNSS SNR measurements. IEEE/ION PLANS 2014. Monterey, California.

[24] Wang, L., Groves, P. D. and Ziebart, M. K. (2015). Smartphone Shadow Matching for Better Cross-street GNSS Positioning in Urban Environments. Journal of Navigation, 68, 411-433, doi 10.1017/S0373463.314000836. Also available from http://discovery.ucl.ac.uk/.

[25] Yozevitch, R. and Ben-Moshe, B. (2015). A Robust Shadow Matching Algorithm for GNSS Positioning, *NAVIGATION*, 62 (2), 95-109.

[26] Wang, L., Groves, P. D. and Ziebart, M. K. (2013). Urban Positioning on a Smartphone: Real-time Shadow Matching Using GNSS and 3D City Models. ION GNSS+ 2013. Nashville, Tennessee. Also available from http://discovery.ucl.ac.uk/.

[27] Groves, P. D., Wang, L., Adjrad, M., and Ellul, C. (2015). GNSS Shadow Matching: The Challenges Ahead, Proceedings of ION GNSS+, Tampa, FL. Also available from http://discovery.ucl.ac.uk/.

[28] Amt, J. H. R., and Raquet, J. F. (2006). Positioning for Range-Based Land Navigation Systems Using Surface Topography. Proceedings of ION GNSS 2006, Fort Worth, Texas.

[29] Adjrad, M and Groves, P. D. (2015b). Enhancing Conventional GNSS Positioning with 3D Mapping Without Accurate Prior Knowledge, Proceedings of ION GNSS+ 2015 conference, Tampa, Florida. Also available from http://discovery.ucl.ac.uk/.

[30] Groves, P. D. and Jiang. Z. (2013). Height Aiding, C/N0 Weighting and Consistency Checking for GNSS NLOS and Multipath Mitigation in Urban Areas, Journal of Navigation, 66, 2013, 653–669. Also available from http://discovery.ucl.ac.uk/.

[31] Ordnance Survey: https://www.ordnancesurvey.co.uk/

[32] RTCA (2006). Minimum Operational Performance Standards for Global Positioning System/Wide Area Augmentation System Airborne Equipment, DO-229D.

[33] Hartinger, H. and Brunner, F.K. (1999). Variances of GPS Phase Observations: The SIGMA-ε Model. GPS Solutions, Vol. 2, No. 4, 35–43.

[34] Dorey, M. (2002). Digital elevation models for intervisibility analysis and visual impact assessment, PhD dissertation, University of Glamorgan, Pontypridd, Wales.

[35] Adjrad, M., Groves, P. D., and Ellul, C. (2015a). Enhancing GNSS Positioning with 3D Mapping, RIN International Navigation Conference 2015, Manchester, UK. Also available from http://discovery.ucl.ac.uk/.

[36] Kidner, D. B. (2003). Higher order interpolation of regular grid digital elevation models, International Journal of Remote Sensing, 24, 315-323.

[37] Press, W. H., Teukolsky, S. A., Vetterling, W. T., Flannery, B. P., and Metcalf, M. (1996), Numerical Recipes – The Art of Scientific Computing (Cambridge: Cambridge University Press).

[38] https://www.u-blox.com/en/product/evk-8evk-m8 (u-blox 8/M8 concurrent GNSS evaluation kits).